LHC Project Note 370

2005-04-12

jaroslaw.fydrych@pwr.wroc.pl

Analysis of thermo-mechanical pipe-strength for the LHC helium relief system and corresponding helium flows following a resistive transition of the magnets

Chorowski Maciej*, Fydrych Jaroslaw*, Riddone Germana**

* Wroclaw University of Technology, Poland
**CERN, AT-ACR

Keywords: helium relief system, cold compressed helium flow

Summary

The LHC cryogenic system will contain of about 100 tons of helium mostly located in underground elements of the machine. The amount of helium stored in the magnet cold masses located in one sector of the LHC machine will be of about 6400 kg. In case of a simultaneous resistive transition (quench) of the magnets of a full sector of the accelerator, the helium will be relieved to a dedicated relief system. The system will comprise header D, quench lines connected to medium pressure tanks, vent line open to environment and accessories. We analyse a dynamic behaviour of the system with respect to its thermo-mechanical properties and overall capacity. Spatial and time distribution of pressure, temperature, velocity, density and flow rates in the system elements are presented. Thermo-mechanical stresses in the critical pipe sections have been calculated.

1. Introduction

The amount of helium stored in the magnet cold masses located in one sector of the LHC machine will be of about 6400 kg. In previous studies (LHC Project Note 77 [4]) a sector quench has been defined as an event that may occasionally occur during a life-time of the machine. In case of this event the magnet cold masses will be protected against pressure increase above acceptable level by superfluid helium safety relief valves (SRV). If pressure inside magnet cryostats reached 17 bar the helium would be vented from cold masses to cold recovery header D. The capacity of header D would not allow to gather all the helium blown from the cold masses after a sector quench. The excess helium would have to be relieved via the pressure valves (PV) and quench lines (QL) to two buffer volumes, each composed of four 250 m^3 medium pressure tanks. There is also a possibility to discharge the helium via safety valve (SV) or bursting disks (BD) to the vent line (VL), which opens directly to the environment. The scheme of the helium relief system is shown in figure 1.

The connections of header D with the lines QL are located in both extremities of the sector, inside the cryogenic interconnection box (QUI), and the return module (RM). The QUI comprises also a connection of header D with VL. The set pressures of the safety elements PV, SV and BD are respectively 6, 9 and 14 bar. If the pressure inside header D exceeds 6 bar the PV will open. If the helium pressure reaches the value of 9 bar then a safety valve (SV)

will open. If the pressure inside header D exceeds 14 bar, one of the two BD will rupture. The hysteresis of PV valve is 2 bar (the valve will close when the pressure in header D decreases to 4 bar) and the hysteresis of SV valve is assumed to be negligible.

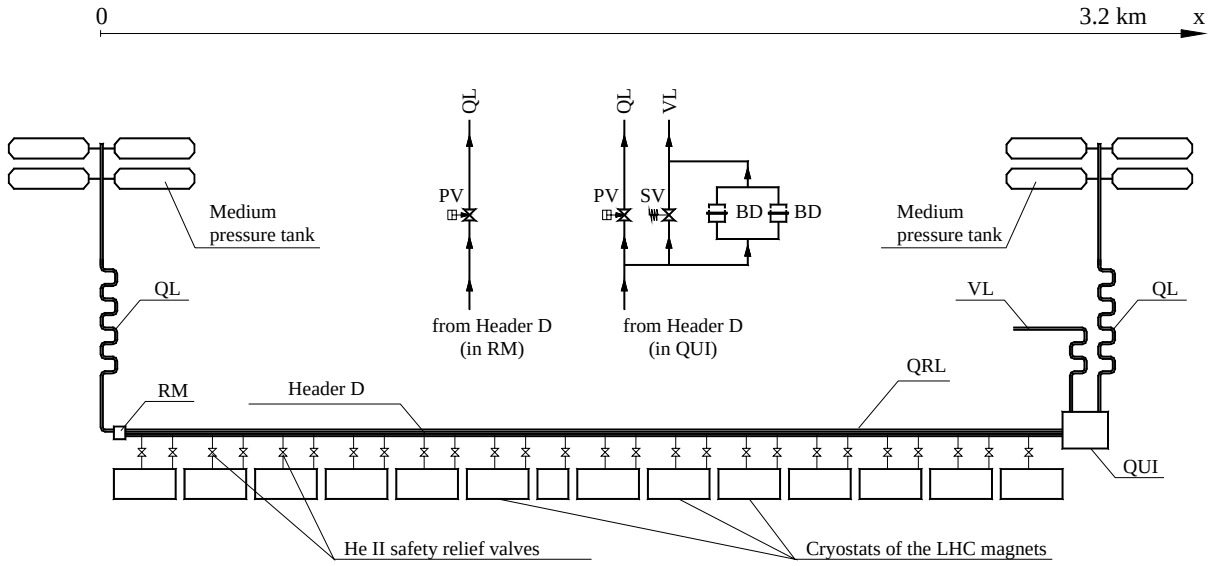

Figure 1 Helium relief system scheme

2. Aim and scope of the analysis

2.1 Aim of the work

The aim of the analysis is to study flow and mechanical operational aspects of the helium relief system composed of header D, QL and VL lines and the accessories, as shown in figure 1. In particular the following issues are considered:

- Helium venting through the quench lines following a sector quench with respect to the line mechanical strength when exposed to thermal and pressure impact loads after the pressure valve opening. This is supposed to be the most critical event for the line QL.

- Helium venting through VL after the bursting disks rupture with respect to the line mechanical strength when exposed to thermal and pressure loads. This is supposed to be the most critical event for the line VL. This flow will appear when the pressure at the extremity of header D in the vicinity of bursting disks increases above the level of 14 bar and the pressure valves PV as well as safety valve SV would not open.

- Pressure evolution inside header D caused by the relief of cold helium from the LHC magnets cryostats after a sector quench and with consideration of the above characterised outflows via QL and VL lines.

2.2 Scope of the work

The analysis is focused on the helium relief system of the LHC sector between the points P7 and P8 (sector 8-7). The scope of the work includes:

- Estimation of helium flow from the magnet cryostats into header D.
- Numerical modelling of helium flow from header D through QL following a sector quench.
- Numerical modelling of helium flow from header D through BDs and VL following a sector quench.
- Numerical analysis of the stresses in the pipe walls.

The results of this analysis can be applied to any other LHC sector.

3. Estimation of helium flow from cold mass to header D

The helium flow into QL (or VL) will be triggered by the pressure growth in header D. After a sector quench a part of the magnetic energy will be dissipated in the helium inside the cold mass and will cause the increase of its temperature and pressure. Based on experimental data gathered from String 1 [4] and String 2 [3] the heat flux to the helium in the cold mass after a sector quench was estimated (Fig. 2). The heat flux will reach the highest value (about 50 MW) during the first second and it will rapidly go down to 3.7 MW. It will then decrease to about 1 MW during a period of about 20 s, and afterwards it will constantly and gradually reduce at much slower rate.

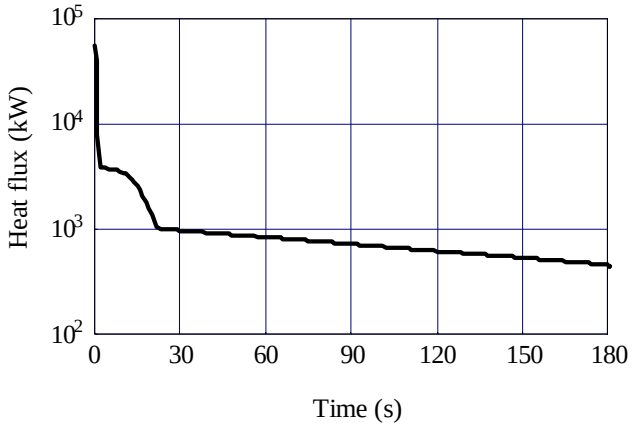

Figure 2 Evolution of heat flux to the cold mass helium

The internal energy U of the helium in the magnets can be calculated from the following equation:

$$U_2(T_2, p_2) = U_1(T_1, p_1) + \int_{t1}^{t2} P(t)dt - h(T_1, p_1) \cdot \Delta m \qquad (1)$$

where P refers to power dissipated in the helium, h is specific enthalpy of helium and Δm denotes the mass of helium that flows out from the magnet cryostats to header D. Equation (1) together with the helium equation of state [7] enables to calculate the helium mass flow rate $q_m = \Delta m/\Delta t$ from the cold mass to header D (Fig. 3a) as well as the helium temperature

and pressure evolutions (Fig. 3b). After 11 s following a sector quench, the helium pressure in cold mass will reach the value of 17 bar and He II safety relief valves will open and will allow helium to flow into header D. The helium mass flow rate will then increase rapidly to about 42 kg/s. During the next 9 s the flow rate will sharply decrease to the value of about 18 kg/s, and afterwards it will further go down, but much more smoothly and gradually.

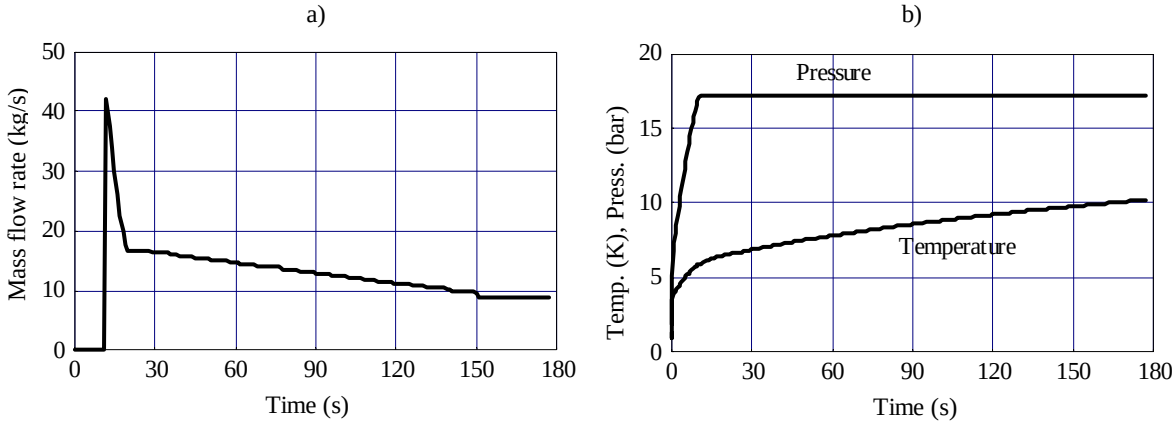

Figure 3 Evolutions of helium mass flow out of the cold mass (a) and helium temperature and pressure in the magnet cryostats after a sector quench (b)

Based on the calculated helium outflow from the cold mass, the helium temperature and pressure evolutions in header D have been calculated taking into account the thermal capacity of header D. The solution (Fig. 4) reveals that the helium temperature inside header D will drop quickly down from 20 K to 10 K during the first 30 s. The lowest value of temperature will be of about 9 K and it will be reached after approximately 90 s after a sector quench trigger. Later the header D temperature will go slightly up following the increase in the cold mass helium temperature – compare Fig. 3.

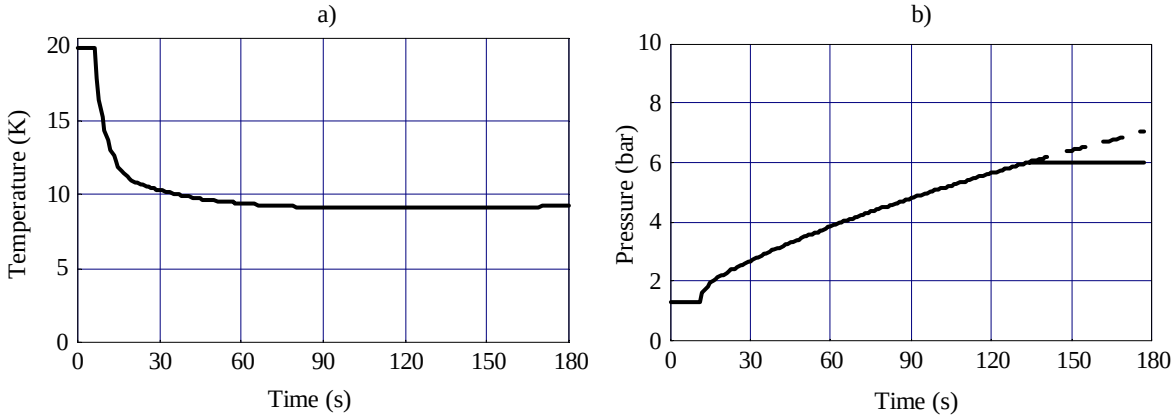

Figure 4 Evolutions of helium temperature (a) and pressure (b) in header D after a sector quench

During the time delay between a sector quench and the opening of PV valves the pressure and temperature inside header D will increase quite uniformly due to a high number of the inlets and their even distribution along the header at each 107 m. At 135 s after a sector quench the pressure in header D will exceed 6 bar, and we assume that both PV valves will open simultaneously. The PV valves will allow the helium to flow out to medium pressure tanks through the QL lines. Because the outlets are located only at the extremities of header D (see Fig. 1) a significant diversification of the helium parameters along header D will occur.

As regards the thermo-mechanical strength of the safety system piping we have identified the most critical events for QL and VL lines. The worst case scenario for the QL thermo-mechanical resistivity is a sudden inflow of cold and compressed helium after full PV valve opening, while in the case of VL it is a sudden inflow of the helium after bursting disk rupture. To find out the helium flow rates and to understand how the helium outflow affects the distribution of the helium parameters in header D both critical flows were investigated numerically.

4. Numerical models of helium flows from header D through QL and VL

Two helium flows have been modelled and solved numerically:

- Helium flow through QL after PV opening (hereafter QL-model),

- Helium flow through VL after BD rupture (hereafter VL-model).

The piping system of the lines QL and VL is complicated [8]. The lines are composed of numerous straight sections composed of the pipes of four different diameters and a number of flow obstructions (valves, reducers and elbows) (Tab. 1).

Table 1. Header D, QL and VL components at sector 8-7

		Pipe		Flow obstruction
		Diameter	Length	
Header D		150 mm	3200 m	-
Point 8	QL	200 mm	325 m	1× pressure valve, DN100, k_v = 240 m^3/h 2 × reducer 200/150 mm 28 × 90 deg elbow 13 × 45 deg elbow
		150 mm	11.6 m	3 × 90 deg elbow
		80 mm	2.2 m	1 × reducer 150/80 mm
		50 mm	1.2 m	1 × reducer 80/50 mm 1 × 90 deg elbow
	VL	200 mm	164 m	1 × safety valve, DN65, k_v = 95 m^3/h 2 × bursting disk, DN 100 1 × reducer 200/150 mm 13 × 90 deg elbow 1 × 45 deg elbow
Point 7	QL	150mm	170 m	Similar to QL at Point 8
		200 mm	600 m	Similar to QL at Point 8

To build the numerical models, we had to straighten hydraulically the lines QL and VL by replacing all the flow obstructions by equivalent lengths of straight pipes [10]. Additionally we replaced four medium pressure tanks with one tank of equivalent volume capacity. The dimensions of header D, QL, VL and the tank are presented in table 2.

Table 2. Geometries and measurements of the components of numerical flow models

Model	Component	Component geometry	Equivalent dimensions		
			Length	Diameter	Volume
QL-model	Header D	Long straight pipe	3200 m	150 mm	28.3 m^3
	Quench line	Long straight pipe	420 m	200 mm	13.2 m^3

	Tank	Cylindrical vessel	35.5 m	6 m	1000 m^3
VL -model	Header D	Long straight pipe	3200 m	150 mm	28.3 m^3
	Vent line	Long straight pipe	200 m	200 mm	6.3 m^3

4.1. Equation and calculation procedure

The numerical models of helium flows from header D through QL and VL lines have been solved in ANSYS 7.1 Code [1], in its Computational Fluid Dynamic module FLOTRAN CFD. The finite element method has been applied to solve the set of the three-dimensional equations of mass, momentum, energy and turbulence transports. Helium mass flows and heat transfers were considered simultaneously. For all numerical simulations FLUID-141 element with axis-symmetry option has been chosen. All flows have been modelled as transient (unsteady), turbulent, thermal and compressible. The applied set of equations is:

- Continuity Equation:

$$\frac{\partial \rho}{\partial \tau} + \frac{\partial(\rho \cdot u_x)}{\partial x} + \frac{\partial(\rho \cdot u_y)}{\partial x} + \frac{\partial(\rho \cdot u_z)}{\partial x} = 0 \tag{2}$$

- Momentum Equations:

$$\frac{\partial \rho u_x}{\partial \tau} + \frac{\partial(\rho\, u_x\, u_x)}{\partial x} + \frac{\partial(\rho\, u_y\, u_x)}{\partial y} + \frac{\partial(\rho\, u_z\, u_x)}{\partial z} =$$
$$\rho\, g_x - \frac{\partial\, p}{\partial x} + Rs_x + \frac{\partial}{\partial x}\left(\mu_e \frac{\partial u_x}{\partial x}\right) + \frac{\partial}{\partial y}\left(\mu_e \frac{\partial u_x}{\partial y}\right) + \frac{\partial}{\partial z}\left(\mu_e \frac{\partial u_x}{\partial z}\right) + Vis_x \tag{3}$$

$$\frac{\partial \rho u_y}{\partial \tau} + \frac{\partial(\rho\, u_x\, u_y)}{\partial x} + \frac{\partial(\rho\, u_y\, u_y)}{\partial y} + \frac{\partial(\rho\, u_z\, u_y)}{\partial z} =$$
$$\rho\, g_y - \frac{\partial\, p}{\partial y} + Rs_y + \frac{\partial}{\partial x}\left(\mu_e \frac{\partial u_y}{\partial x}\right) + \frac{\partial}{\partial y}\left(\mu_e \frac{\partial u_y}{\partial y}\right) + \frac{\partial}{\partial z}\left(\mu_e \frac{\partial u_y}{\partial z}\right) + Vis_y \tag{4}$$

$$\frac{\partial \rho u_z}{\partial \tau} + \frac{\partial(\rho\, u_x\, u_z)}{\partial x} + \frac{\partial(\rho\, u_y\, u_z)}{\partial y} + \frac{\partial(\rho\, u_z\, u_z)}{\partial z} =$$
$$\rho\, g_z - \frac{\partial\, p}{\partial z} + Rs_z + \frac{\partial}{\partial x}\left(\mu_e \frac{\partial u_z}{\partial x}\right) + \frac{\partial}{\partial y}\left(\mu_e \frac{\partial u_z}{\partial y}\right) + \frac{\partial}{\partial z}\left(\mu_e \frac{\partial u_z}{\partial z}\right) + Vis_z \tag{5}$$

- Energy Equation:

$$\frac{\partial}{\partial \tau}\left(\rho\, c_p\, T_{st}\right)+\frac{\partial}{\partial x}\left(\rho\, u_x\, c_p\, T_{st}\right)+\frac{\partial}{\partial y}\left(\rho\, u_y\, c_p\, T_{st}\right)+\frac{\partial}{\partial z}\left(\rho\, u_z\, c_p\, T_{st}\right)= \\ \frac{\partial}{\partial x}\left(\lambda_t\,\frac{\partial T_{st}}{\partial x}\right)+\frac{\partial}{\partial y}\left(\lambda_t\,\frac{\partial T_{st}}{\partial y}\right)+\frac{\partial}{\partial z}\left(\lambda_t\,\frac{\partial T_{st}}{\partial z}\right)+W^V+E^k+Q_V+\Phi_{dis}+\frac{\partial p}{\partial \tau} \tag{6}$$

The turbulence was simulated with the Standard k-ε Model, described by the following equations:

- Turbulent Kinetic Energy Equation:

$$\frac{\partial \rho K}{\partial \tau}+\frac{\partial\left(\rho\, u_x\, K\right)}{\partial x}+\frac{\partial\left(\rho\, u_y\, K\right)}{\partial y}+\frac{\partial\left(\rho\, u_z\, K\right)}{\partial z}=\frac{\partial}{\partial x}\left(\frac{\mu_t}{\sigma_k}\,\frac{\partial K}{\partial x}\right)+\frac{\partial}{\partial y}\left(\frac{\mu_t}{\sigma_k}\,\frac{\partial K}{\partial y}\right)+\frac{\partial}{\partial z}\left(\frac{\mu_t}{\sigma_k}\,\frac{\partial K}{\partial z}\right)+ \\ \mu_t\Phi-\rho\,\varepsilon+\frac{C_4\,\beta\,\mu_t}{\sigma_t}\left(g_x\frac{\partial T}{\partial x}+g_y\frac{\partial T}{\partial y}+g_z\frac{\partial T}{\partial z}\right) \tag{7}$$

- Dissipation Rate Equation:

$$\frac{\partial \rho \varepsilon}{\partial \tau}+\frac{\partial\left(\rho\, u_x\, \varepsilon\right)}{\partial x}+\frac{\partial\left(\rho\, u_y\, \varepsilon\right)}{\partial y}+\frac{\partial\left(\rho\, u_z\, \varepsilon\right)}{\partial z}=\frac{\partial}{\partial x}\left(\frac{\mu_t}{\sigma_k}\,\frac{\partial \varepsilon}{\partial x}\right)+\frac{\partial}{\partial y}\left(\frac{\mu_t}{\sigma_k}\,\frac{\partial \varepsilon}{\partial y}\right)+\frac{\partial}{\partial z}\left(\frac{\mu_t}{\sigma_k}\,\frac{\partial \varepsilon}{\partial z}\right)+ \\ C_{1\varepsilon}\mu_t\,\frac{\varepsilon}{k}\Phi_{dis}-C_2\rho\,\frac{\varepsilon^2}{k}+\frac{C_\mu\left(1-C_3\right)\beta\;\rho K}{\sigma_t}\left(g_x\frac{\partial T}{\partial x}+g_y\frac{\partial T}{\partial y}+g_z\frac{\partial T}{\partial z}\right) \tag{8}$$

For helium property calculations the FLOTRAN gas model has been applied, and the following formulas have been used:

- for density:

$$\rho=\rho_0\cdot\frac{T_0}{T}\cdot\frac{p}{p_0} \tag{9}$$

- for viscosity:

$$\mu=\mu_0\cdot\frac{T_0+C_{\mu 1}}{T+C_{\mu 1}}\cdot\left(\frac{T_0}{T}\right)^{1.5} \tag{10}$$

- for conductivity: ,

$$\lambda=\lambda_0\cdot\frac{T_0+C_\lambda}{T+C_\lambda}\cdot\left(\frac{T_0}{T}\right)^{1.5} \tag{11}$$

- for specific heat:

$$c_p = const \tag{12}$$

Within the considered temperature and pressure ranges, the differences between the real helium property values and the values obtained from the applied gas model can be neglected. The comparisons of the calculated values according formulas 9 to 12 with the helium property values obtained from HePak ver. 3.4 [7] are presented in appendix A.

4.2 Helium flow through QL

4.2.1 QL-model description

The QL-model describes the helium flow from header D into the tanks through a quench line. The geometry of this model is presented schematically in Figure 5. Header D and QL are considered as straight long pipes. The QL outlet leads into one big tank. The dimensions of QL-model components are presented in Table 2. Header D and QL pipe are connected by valves, which fully and fast open when the pressure inside the header exceeds 6 bar.

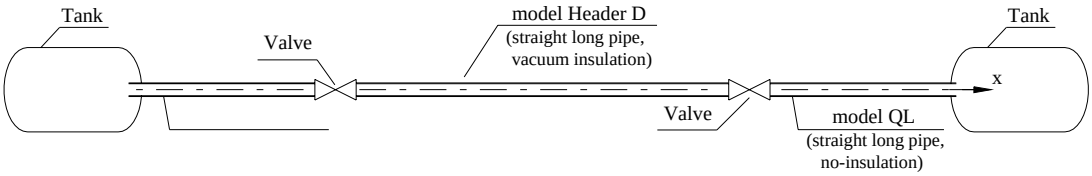

Figure 5 Scheme of the QL-model geometry

The resolution of transient numerical model with complex geometry is extremely time-consuming. Therefore, for shortening the time of calculation a two-dimensional flow area was constructed and axis-symmetry option was applied. The flow area reflected a half of the longitudinal section of header D, QL and tank. The entire flow area was meshed into almost 4800 FLUID-141 elements.

On all outer lines of the flow area, the CFD and thermal boundary conditions were applied. On all lines which stood for walls of the pipes and tank we applied a no-slip condition (stationary wall), whereas on the line that represented the axis we applied a symmetry boundary condition. On the header D wall there was constant temperature 9 K applied, while on the walls of QL and a tank – free convection condition with film coefficient α = 15 W/m^{2}K and bulk temperature 300 K was applied. On all nodes of the flow area the specified initial conditions were applied as well. These conditions simulated the helium properties at the beginning of the analysed flow. For nodes in internal area of header D we applied the following initial helium property values: T_i = 9 K and p_i = 6 bar, whereas for internal area of QL and a tank: T_i = 300 K and p_i = 1 bar. Because of the complex geometry of the model (high difference between the lengths and diameters of the model components), great number of elements and strong time dependence, only the first 10 seconds of the flow were calculated.

4.2.2 QL-model results

The results of the QL-model are presented in Figures 6–8. Figures 6 and 7 show the helium property distributions along header D and line QL respectively, for 6 time periods: 0, 2, 4, 6, 8 and 10 s after PV opening. The time period is sufficient to calculate the maximum stresses in the pipes.

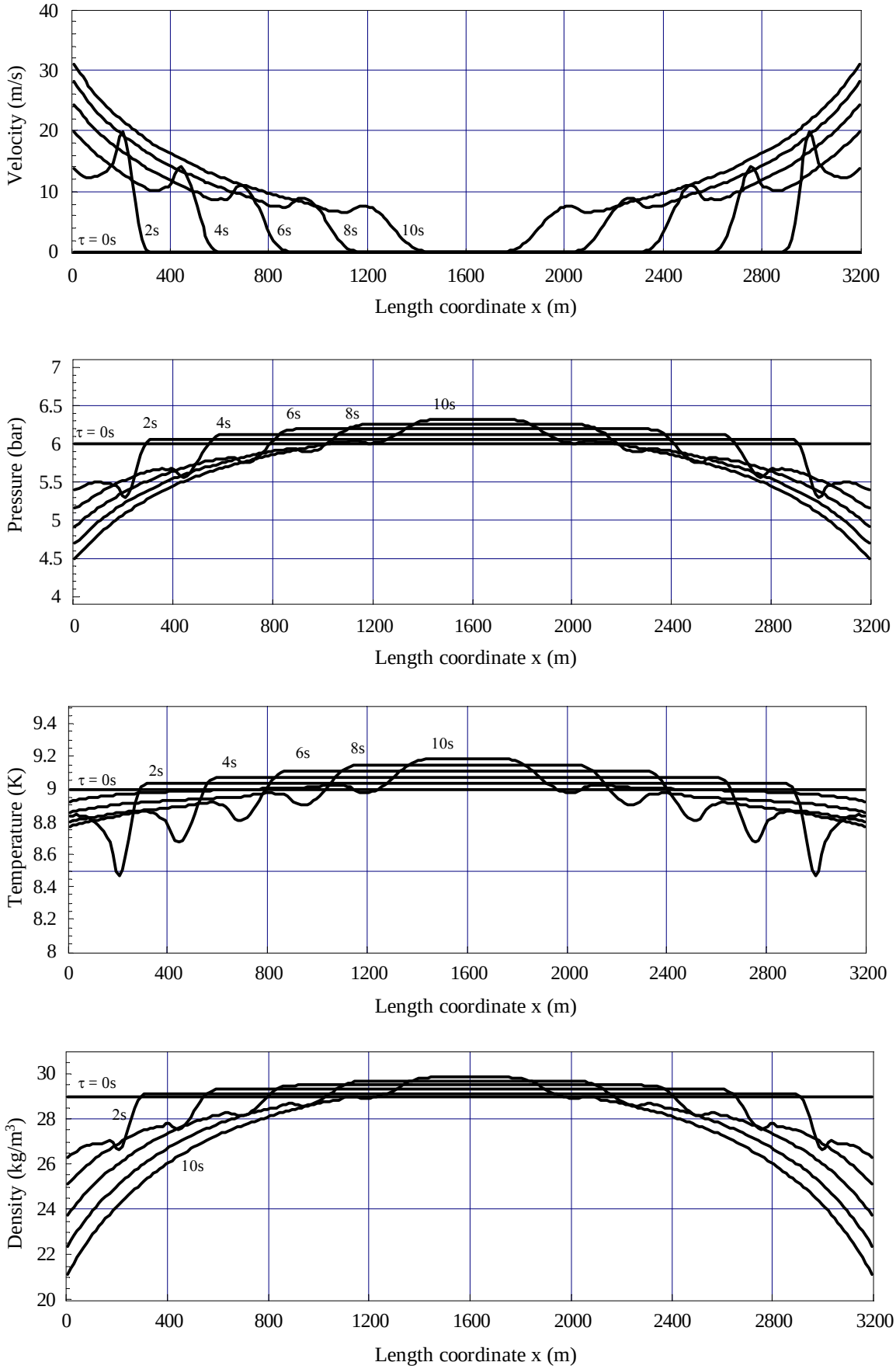

Figure 6 Helium flow and thermodynamic parameter distributions along header D after both PV opening

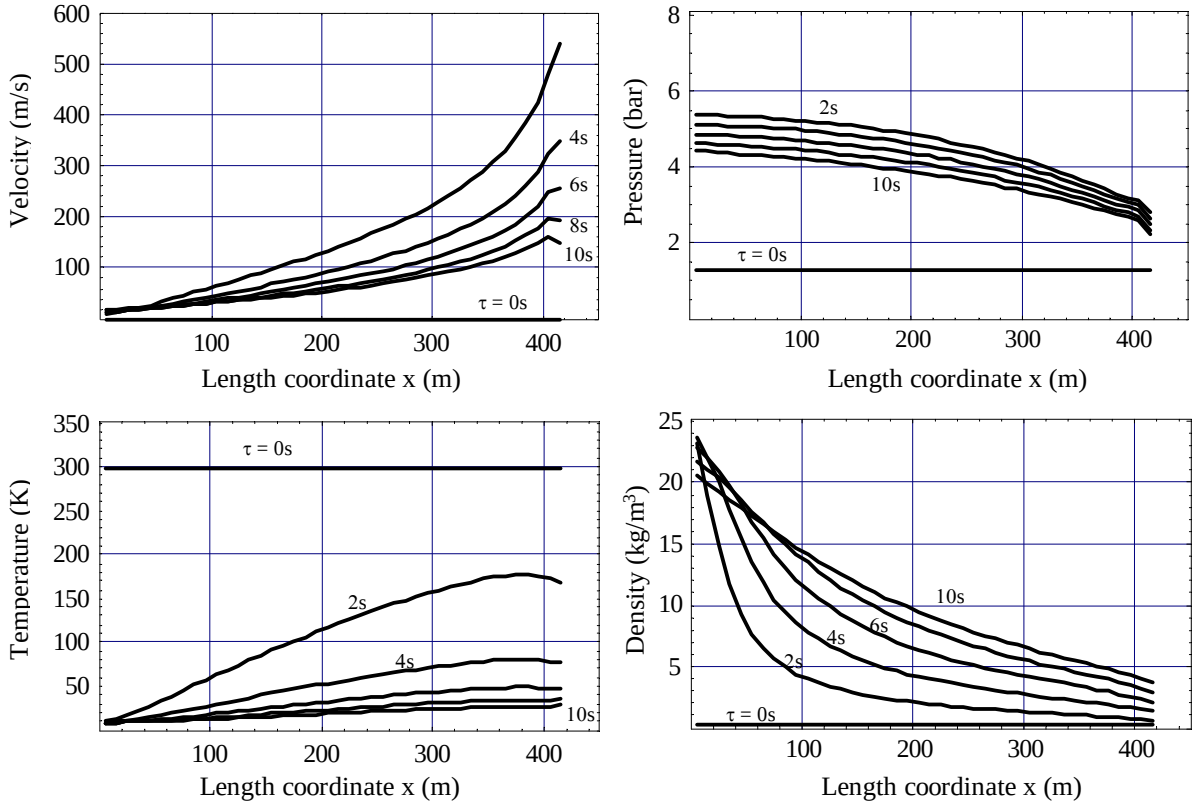

Figure 7 Helium flow and thermodynamic parameter distributions along QL after PV opening

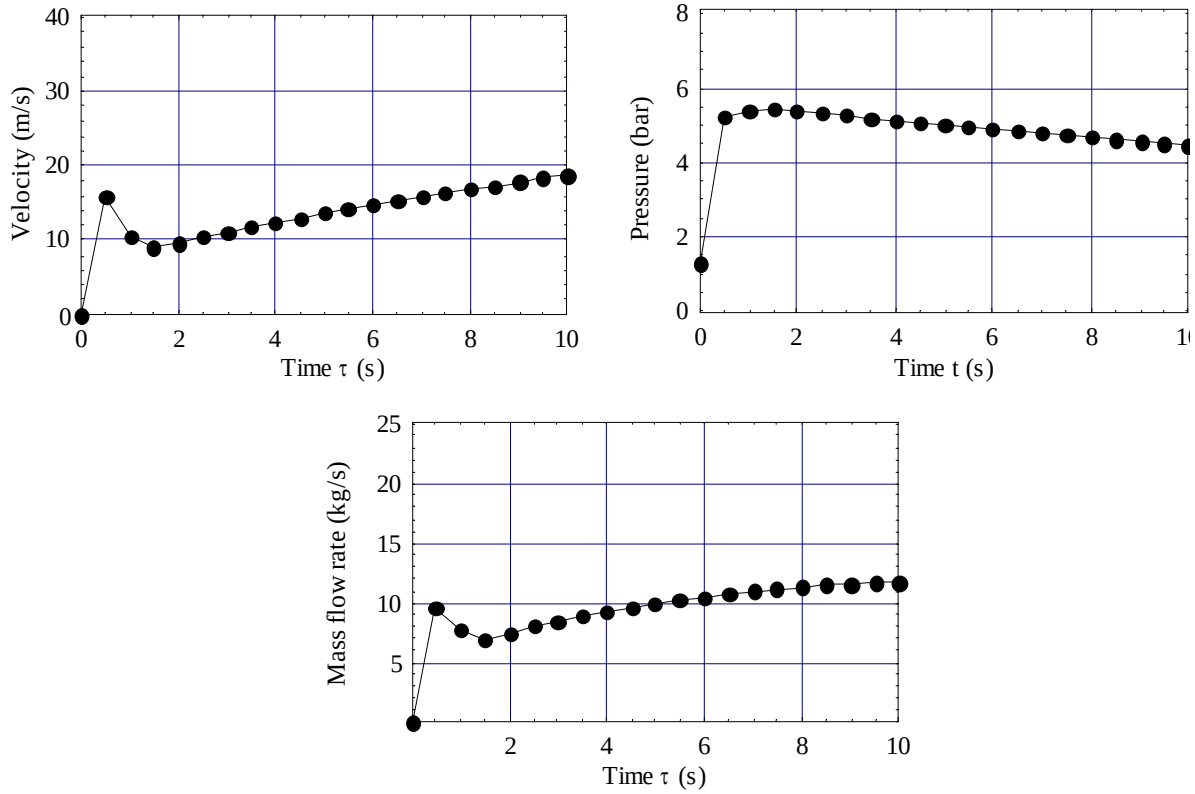

Figure 8 Helium parameter evolutions at the QL inlet after PV opening

The distributions of the helium parameters along header D are significantly diversified (see fig. 6). The pressure, temperature and density distribution curves have different shapes. The values of these parameters are decreasing at header extremities and slightly increasing at its central part. This increase is due to continuous helium inflow from cold masses to the header. The wave of the small disturbance of the properties moves along header D with a sound speed of about 220 m/s, while higher disturbance move much slower, about 160 m/s. During the first 10 seconds of the flow the pressure at the header extremities decreases from 6 to 4.5 bar. Helium temperature at header D decrease as a result of adiabatic decompression but the changes are not very significant (below 0.6 K).

The values of helium velocity in QL (fig. 7) are much greater then in header D. At the beginning of the flow, at the QL outlet into the tank, the velocity reaches almost 550 m/s. As soon as the cold helium reaches the QL outlet, the velocity and temperature drop to significant lower values.

The evolutions of helium velocity, pressure and mass flow rate at the QL inlet section are shown in figure 8. Mass flow rate, as well as pressure and velocity, react quickly to PV opening and rises up to 9.6 kg/s at first 0.5 sec. Then the mass flow rate decreases to 7 kg/s, and after it rises quite gradually over 12 kg/s. The sudden growth and drop of velocity and flow rate values are caused by the value of pressure difference at the beginning of the flow and by heat flux to cold helium.

Because there are two QL at both extremities of header D the expected mass flow rate of helium escaping from the header will be two times higher then the values shown in fig. 8. It reveals that both QL are able to accumulate helium with the maximum flow rate of about 14-24 kg/s. According to earlier estimation PV will open after 135 s following a sector quench. Then the mass flow rate of the helium flowing into header D will be lower then 11 kg/s (see Fig. 3a) and it always will be lower than the potential helium mass outflow rate.

When the helium flow from the header starts, the pressure will suddenly decrease by more then 0.5 bar in the vicinity of the header extremities (Fig. 6). On the other hand, due to continuous helium flow from cold mass, the pressure in the middle region of header D will slightly increase and reach 6.3 bar after 10 s. The comparison of the rate of pressure increase caused by helium inflow to header D to the rate of pressure decrease due to helium outflow from the header, shows that after about 11-12 s the pressure in this region will be almost a constant value.

According to the pressure evolution shown in Figure 8 the helium pressure at the QL, after rapid increase to the value 5.6 bar, will slowly and gradually drop to 4.5 bar after 10 s. It is necessary to mention that in the real relief system, if the helium outflow lasts long enough, the pressure will stop dropping and after a certain period it will start increasing. Then the pressure in header D, as well as in QL and in the tanks will be able to exceed 6 bar. Helium will flow through QL to medium pressure tanks until the pressure inside header D near PV valves is higher then 9 bar. If the pressure exceeds 9 bar, then the SV will open and the excess helium will be vented through the VL to the environment.

4.3 Estimation of the final mass capacity of the safety system

To estimate the amount of the helium which would be accumulated in the safety system we calculated the helium remaining inside the cold mass, header D, both QL and all medium pressure tanks if a sector quench appeared and the helium parameters attained the maximal final values. With this approach we assumed that pressure inside header D reaches the value slightly lower then 9 bar and SV remains closed. The helium masses that could

remain inside the main components of the helium recovery system and the maximal final values of helium pressures and temperatures are presented in Table 3.

Table 3 Helium masses that can be accumulated in the main components of the helium recovery system after a sector quench

	Volume m^3	Condition		Helium density kg/m^3	Helium mass kg
		Pressure bar	Temperature K		
Cold masses	43	17	30	26.1	1123
Header D	59	9	12	40.7	2402
QL	20	9	300	1.44	29
Medium pressure tanks	2000	9	300	1.44	2877
				Total mass	6431

The total mass of the helium that can be gathered inside the safety system is equal to 6431 kg and is slightly bigger then the whole amount of the helium located in one sector of the LHC machine (6400 kg). This shows that, if a sector quench appears the whole amount of helium remains inside dedicated helium recovery system. Therefore, the SV will stay close during all time after a sector quench. The valve would open only if PV do not work properly and helium cannot flow from header D to medium pressure tanks.

It would be recommended to increase a set pressure of SV to 10 bar to achieve additional capacity of the system of about 500 kg. This increase of set pressure would create a 8% redundancy in the helium relief system.

Although the total amount of the helium that is now foreseen to be gathered in the medium pressure tanks (Table 3) is twice the amount analysed in the LHC Project Note 119 [5], the tanks will not be exposed to non-acceptable thermo-mechanical stresses. According to the Fig. 7 the density of the helium flowing into the tanks is 20 times lower then assumed in [5]. It will result a much slower cooling down of the tanks wall, due to a lower convection coefficient. The distribution of the wall temperature will be uniform without any local drops. Taking into consideration the double amount of the helium that will be finally stored in the tanks, the maximum drop of wall temperature will not exceed 16 K (instead of 8 K in [5]). Therefore the tank wall temperature will not decrease below acceptable level of 223 K.

4.4 Helium flow through VL

The helium flow through VL will happen only if PV do not open in spite of pressure growth above acceptable level. With respect to the mechanical strength of VL, the worst case of helium flow through the line would happen after BD rapture, without prior SV valve opening. This flow will occur only if both PV and SV do not work properly and the helium pressure inside header D exceeds 14 bar. The VL would be subjected to the worst thermo-mechanical loads. Therefore we focused on the simulation of flow through VL after BD rupture.

4.4.1 VL- model description

The VL-model describes the flow from header D to the environment through VL after BD rupture. The geometry of the model is shown schematically in Figure 9. The model considers header D and VL straighten hydraulically to its equivalent length of 200 m. The

dimensions of VL-model components are presented in Table 2. Header D and VL are connected by a valve which simulates the bursting disk. The valve opens rapidly when the pressure inside the header exceeds 14 bar and then stays open regardless of the pressure inside header D. After the valve opening the helium will flow through VL to atmosphere (air conditions: p = 1 bar and T = 300 K).

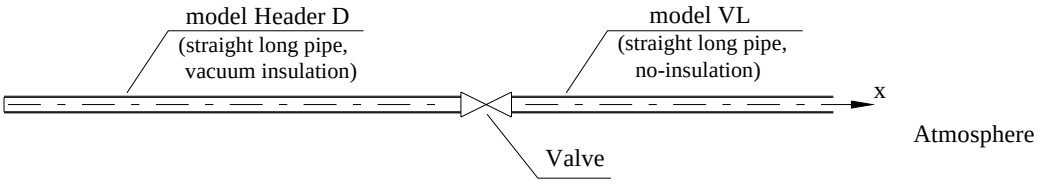

Figure 9 Scheme of the VL-model geometry

For shortening the time of calculation a two-dimensional flow area was constructed and axis-symmetry option was applied. The flow area represented a half of the longitudinal section of header D and VL. The entire flow area was meshed into 1640 FLUID-141 elements.

On header D wall constant temperature T = 12 K and no-slip condition were applied, while on the VL wall convection with film coefficient α = 15 W/m^{2}K and bulk temperature 300 K, and zero velocity condition were applied. On all nodes of the flow area the specified initial conditions were imposed similarly as in the QL-model. Initial temperature inside header D was T_i = 12 K, whereas initial pressure p_i = 14 bar. For the nodes of the VL area we applied temperature T_i = 300 K and absolute pressure p_i = 1 bar.

4.4.2 VL -model results

The results of the VL-model are presented in Figures 10-12. Figure 10 shows the distributions of helium velocity, pressure, temperature and density along header D. Due to higher initial pressure inside header D and shorter length of VL the velocity at header D outlet reaches higher values then in the QL-model. At 10 s after BD rupture the velocity exceeds 95 m/s. After the same time at the right extremity of header D helium pressure decreases from 14 bar to almost 5 bar. Simultaneously, at the left side of the header the pressure is slightly increasing. The rate of pressure increase is much lower then in the QL-model. After 10 s following BD rupture the pressure increase is equal to 0.12 bar. According to Fig. 10 the pressure decrease caused by helium flow in the outlet direction can be expected after 20-24 s. Therefore the maximal pressure increase will not exceed 0.3 bar.

The higher initial pressure also affects the helium density. Before BD rupture the density is equal to 64.1 kg/m^3 in whole header D. Then, when the flow starts, the density of helium located near the VL inlet drops gradually to 21 kg/m^3.

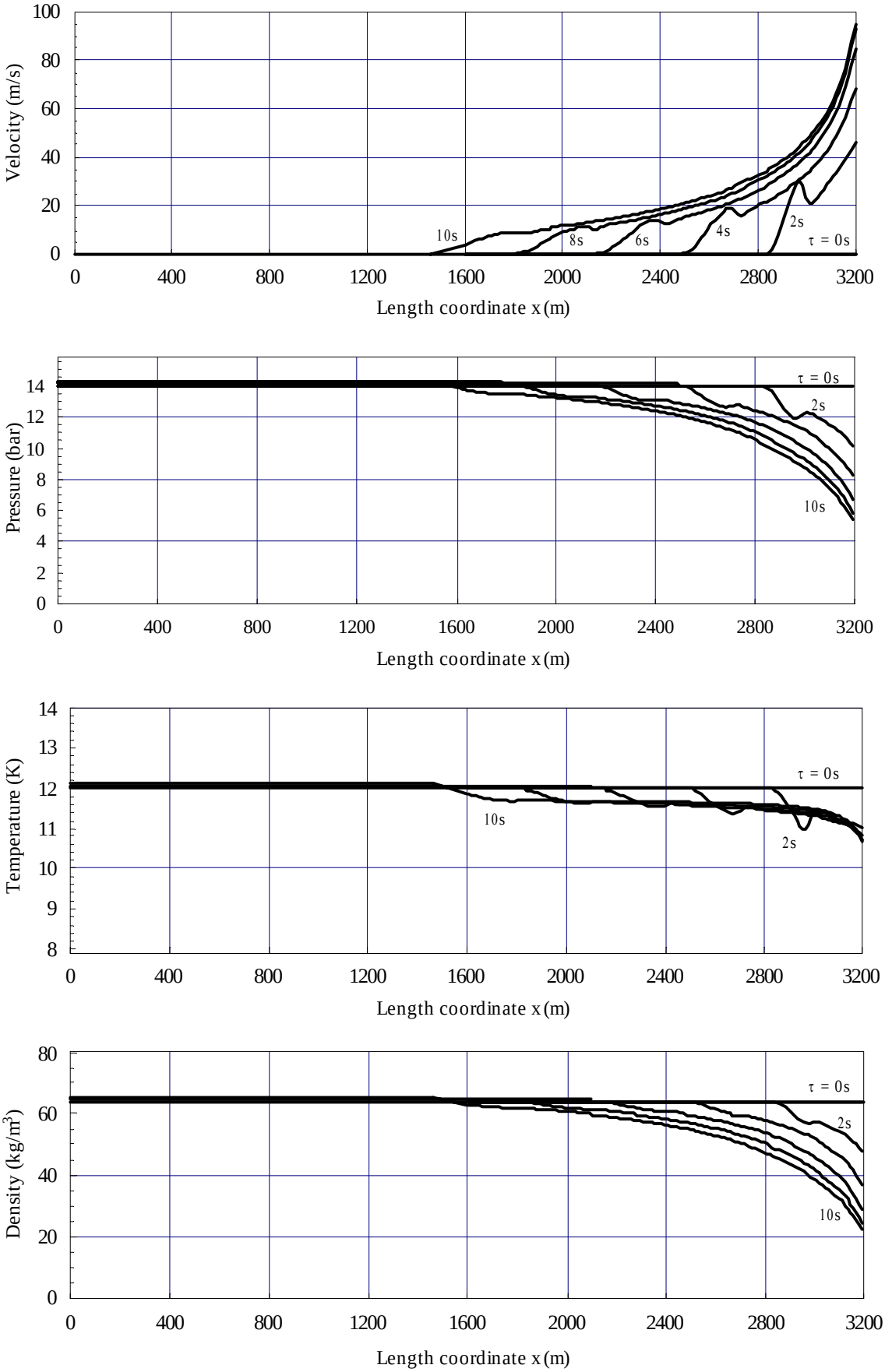

Figure 10 Helium flow and thermodynamic parameter distributions along header D after BD rupture

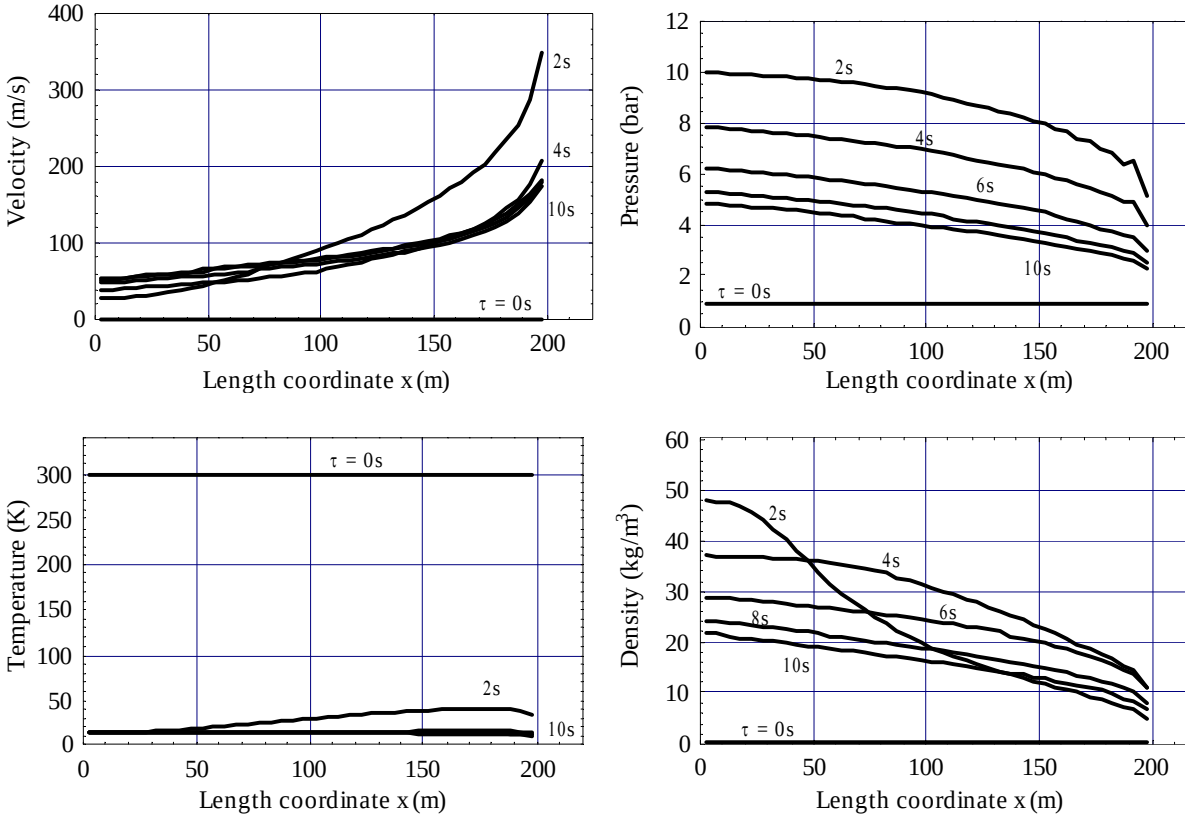

Figure 11 Helium flow and thermodynamic parameter distributions along VL after BD rupture

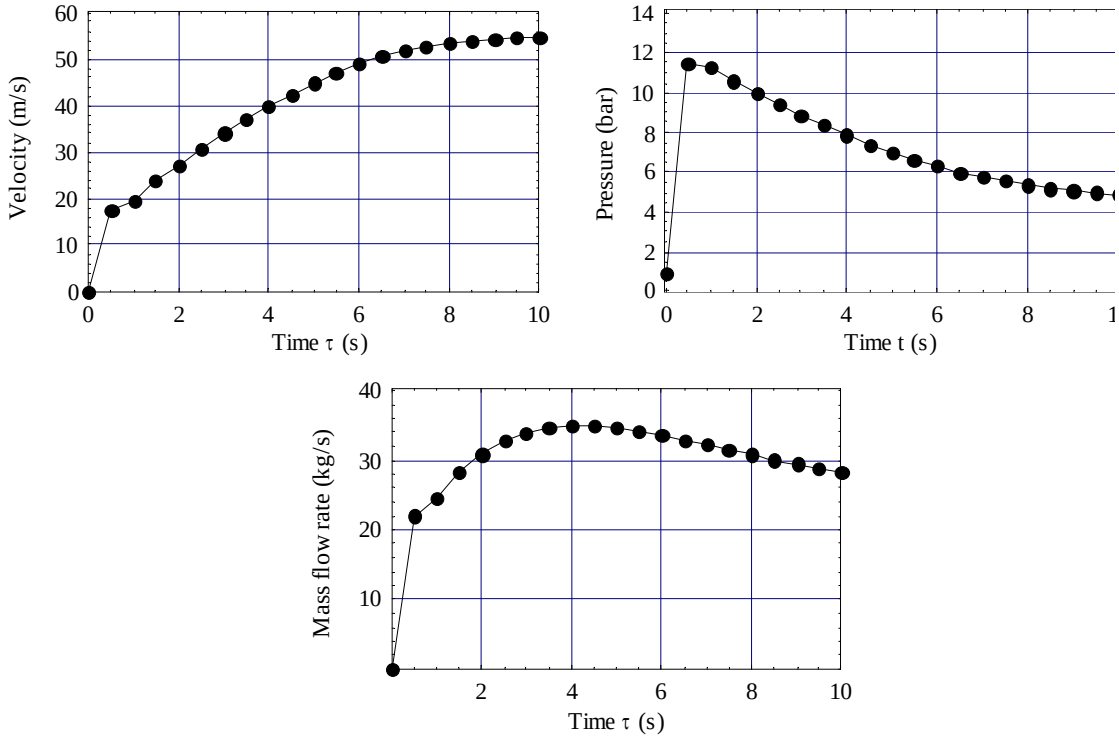

Figure 12 Helium parameter evolutions at the VL inlet after BD rupture

When compared the QL and VL models, the differences in the helium distribution in the QL and VL lines are significant (see Fig. 11). The temperature of helium flowing through VL drops fast. Velocities at the VL outlet are also lower for the first seconds of the flow. This is also due to the higher initial pressure and shorter length of VL. Cold helium vapour is able to fill all VL pipe much faster. The cold helium appears at the VL outlet already 2-3 s after SV opening.

The evolutions of helium properties and its mass flow rate at the VL inlet cross section for VL-model are shown in Figure 12. Velocity gradually rises to 55 m/s, while pressure, after a sudden jump to 11.4 bar, drops below 5 bar after 10 s of flow. Helium mass flow rate at the beginning rapidly rises to 22 kg/s and then the increase becomes weaker. The flow rate reaches 35 kg/s at 4 s after BD rupture, and afterwards it slowly lowers to 28 kg/s after 10 s.

5. Numerical study on the thermo-mechanical stresses in pipe wall material

5.1. Description of the pipe strength model

Both QL and VL, especially in their inlet sections, can be subjected to sudden contact with cold and compressed helium. Therefore, because of the thermal shrinkage of pipe wall material and due to high pressure loads, thermo-mechanical stresses can occur. To calculate the values of these stresses and to analyse pipe strength aspects the finite element method (FEM) has been applied.

The most critical case for all pipes will happen, when after a sector quench both PV and SV do not work properly. Then the pressure inside header D can exceed 14 bar and the BD can rupture. As a result of the BD rupture the cold helium vapour will be released to the warm VL. According to numerical simulation of helium flow through VL after BD rupture the pressure in the VL inlet after a half second of flow will be equal to 11.4 bar, and the temperature to about 12 K. Any other case will represent much less extreme initial condition. For this reason, only the most critical case was analysed.

The cross section of the pipe considered in the model was DN200×3mm. The inner wall of the pipe was subjected to sudden contact with cold and compressed helium vapour. The helium temperature was equal to 12 K and the pressure did not exceed 11.4 bar. The scheme of the pipe strength model is shown in figure 13.

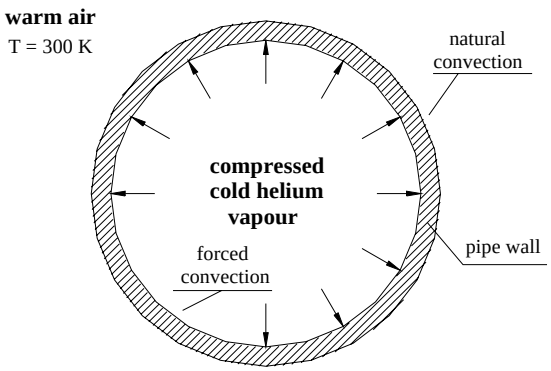

Figure 13 Scheme of the pipe strength model

Because the cold helium vapour will be rapidly flowing through the pipe we assumed forced convection on the inner pipe wall surface with bulk temperature T = 12 K. The value of convective heat transfer coefficient according to calculation method presented in [2] can be equal as much as 2400 W/m^{2}K.

The model pipe wall surface was surrounded by air at temperature of 300 K and under normal pressure. On this surface we assumed free convection with bulk temperature T = 300 K and film coefficient α = 15 W/m^2 K. The initial temperature of the pipe was equal to 300 K.The model mesh is based on 640 divisions in the circumferential and 20 divisions in the wall thickness direction. The model of the pipe wall material simulated all significant thermo-mechanical properties of austenitic stainless steel AISI 304L (the material of the VL). The model also considered the dependence of thermal conductivity, thermal expansion and Young modulus on temperature in the range between 4 and 300K (see appendix B).

5.2 Pipe strength model results

The obtained results are presented in Figures 14 and 15. Figure 14 shows the temperature distributions along the pipe wall thickness after cold helium inflow. The temperature decreases quickly but quite gradually. After 20 seconds the inner pipe wall surface temperature falls down to 19 K. The temperature distributions along wall thickness are rather flat: the difference between inner and outer surface temperatures does not exceed 26 K.

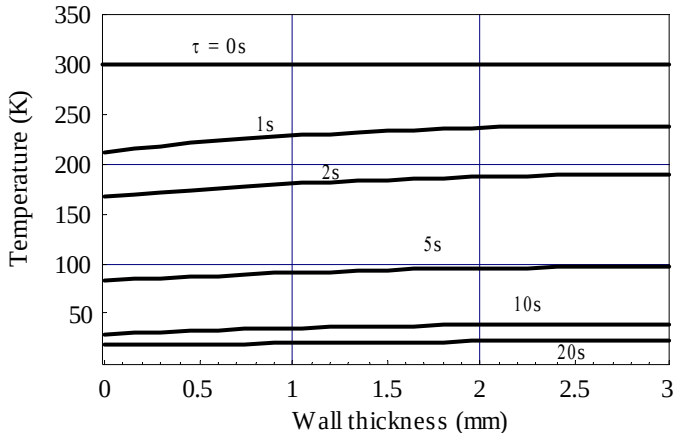

Figure 14 Temperature distributions along the wall thickness of the model pipe after BD rupture

Figure 15 shows von Mises stress distributions along the wall thickness. During few seconds at the beginning of cold helium flow the stresses are higher near the inner surface. Then after 6-8 s the stresses are higher in the region near the outer surface. The stress values are not very high and they do not exceed the 120 MPa.

For the austenitic stainless steel AISI 304L at 300 K the values of yield and tensile strength are equal 210 MPa and 500 MPa, respectively. Furthermore, the strength values increase gradually for lower temperatures to 490 MPa for yield strength, and to 1450 MPa for tensile strength (see Fig. B3 in appendix B).

The pipe strength model results presented in Fig. 15 show that the stresses in the pipe wall material will be at most twice lower then the yield strength.

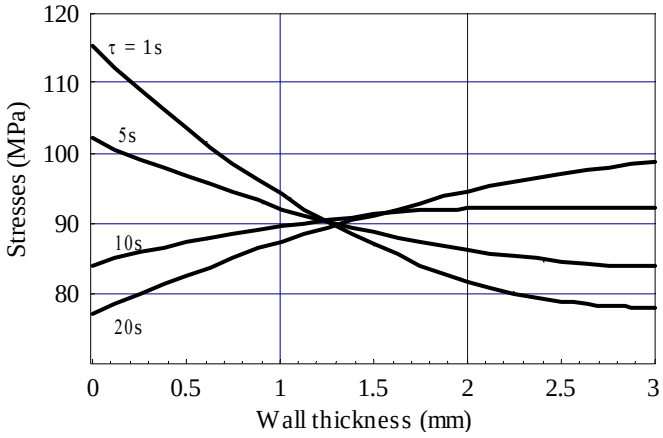

Figure 15 Stress distributions along the wall thickness of the model pipe after BD rupture

6. Effect of dynamic pressure impact in QL and VL elbows

The effect of cold helium pressure impact can occur in the QL and VL elbows located close to QUI. The highest impact can be expected in the first VL elbow after BD rupture. Then the helium will have the highest density (ρ = 65 kg/m^3) and the pressure caused by the flow will reach the highest value (14 bar). After BD rupture the helium will be suddenly released to the VL with velocity u not exceeding 55 m/s (see Fig. 15). The helium impact into the elbow inner wall will cause a dynamic force F.

The momentum of the cold helium flowing inside the elbow is given by equation 13,

$$M = \rho \frac{\pi d^2}{4} \Delta s \, u \tag{13}$$

where d is a pipe diameter (150 mm) and Δs refers to the distance crossed by the helium through the period of time $\Delta \tau$:

$$\Delta \tau = \frac{\Delta s}{u} \tag{14}$$

The maximum value of the force F results from the assumption of a total de-acceleration of the cold helium passing through the elbow:

$$F = \frac{M}{\Delta \tau} = \rho \frac{\pi d^2}{4} u^2 \tag{15}$$

and it will be equal 3475 N. Taking into account that the elbow inner wall surface is equal to 8.32 dm^2, it must be noticed that the force can cause the additional dynamic pressure of 41.8 kPa, which is only 2.1 % of the VL nominal pressure.

7. Proposal of the experimental validation of numerical model results

The presented study of safety and operational aspects of the helium relief system is based on the numerical calculation of flows through header D, QL and VL, and on the numerical calculation of pipe thermo-mechanical strength. To validate the numerical some experimental verifications should be carried out.

The main component of the analysis which is burdened with some extent of uncertainty is the numerical modelling of helium flow through the system. The complex geometry of the relief system, the immense ratio of pipe length versus diameter (exceeding 21000), transient and turbulent character of the flows and strong temperature influence present the essential causes of the high level of uncertainty. Therefore to verify the obtained flow calculation results we propose to carry out some simple physical experiments.

The schematic diagram of the test rig for the experimental verification of the numerical calculation of helium flow through QL and VL is shown in Figure 16. The pipes that simulate QL and VL are wrapped in coils to reduce the dimensions of the test rig. At the inlets of both pipes special connectors enable to connect the pipes with a cryogenic vessel.

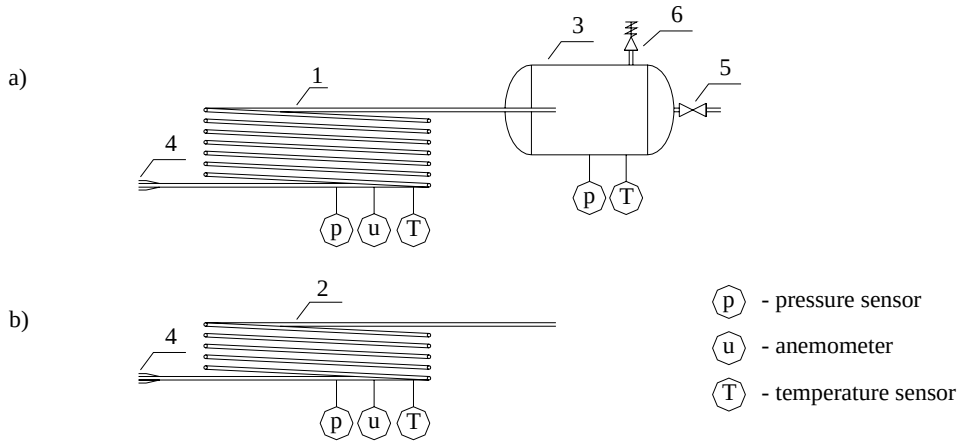

Figure 16 The test rig schematic diagram; 1 – model of QL, 2 – model of VL, 3 – tank, 4 – cryogenic vessel-pipe connector, 5 – blow-off valve, 6 –safety valve

Both pipes and tank can be equipped with temperature and pressure sensors as well as with anemometers. This instrumentation will enable to measure temperature, pressure and velocity evolutions.

During the experimental investigation cold cryogen vapour (helium or nitrogen) can be release from a vessel into a model QL or VL and then pressure, velocity and temperature evolutions can be measured in some chosen cross sections. The obtained experimental results will allow the verification of the results of numerical calculations.

8. Conclusions

The main conclusions of this study are listed hereafter:

1. The capacity of the main components of the relief system (header D, QL and medium pressure tanks) is enough to accommodate all the helium expelled from the cold mass after a sector quench. Then the helium pressure inside these components can

reach almost 9 bar. A redundancy of about 8 % of the relief system can be achieved by increasing the SV valve set pressure to 10 bar.

2. The inlet sections of QL and VL can be subjected to the most critical thermo-mechanical loads. After cold and compressed helium inflow to one of these pipes the stresses in pipe wall material will not exceed 120 MPa which is twice lower then the nominal yield strength of the applied material (240 MPa).

3. The maximum value of a dynamic impact force resulting from sudden helium inflow into the first elbow of the VL will not exceed 3475 N and will not create any danger to the construction.

4. Helium inflow to header D from cold mass can be investigated with lumped-parameter models because there is a big number of connectors between the header and magnet cryostats and their layout along the header is rather uniform. The helium parameters during this inflow will distribute almost uniformly.

5. Specific character of the LHC relief system geometry, especially the immense ratio of pipe length versus diameter (exceeding 21000), can cause the strong non-uniform distributions of helium parameters along the pipes during helium flow from header D through QL or VL.

6. The numerical analysis of flow from header D to QL and VL should be verified and validated experimentally. The obtained calculated results are burdened with some extent of uncertainty because of the complex geometry of the relief system, the immense ratio of pipe length versus diameter, transient and turbulent character of the flows and strong temperature influence on helium parameter evolutions.

Nomenclature

$C_{1\varepsilon}$ – multiplier of shear rate generation term
C_2
C_3 – multiplier of dissipation source term
C_4 – buoyancy dissipation
C_λ – multiplier of the buoyancy term of turbulent kinetic energy equation
C_μ – conductivity formula constant – turbulent viscosity update constant
$C_{\mu 1}$ – Sutherland's constant
c_p – specific heat
E^k – kinetic energy
F – force
g – acceleration
h – specific enthalpy
K – turbulent kinetic energy
K_V – valve flow coefficient,
m – mass
M – momentum
p – pressure
P – power
Q_V – volumetric heat source
q_m – mass flow rate
R – gas constant,
Rs – distributed resistance
s – distance
T – temperature
u – velocity
U – internal energy
W^V – viscous work term
V_{HD} – volume capacity of header D
V_{vis} – viscous loss term
x, y, z – Cartesian coordinates

a – convection film coefficient
β – thermal expansion coefficient
ε – turbulent kinetic energy dissipation rate
Φ – viscous heat generation term
Φ_{dis} – viscous dissipation
κ – isentropic exponent
λ – thermal conductivity
μ – dynamic viscosity
μ_e – effective viscosity
μ_t – turbulent viscosity
ρ – density
σ_k – Schmidt number for the turbulent kinetic energy
σ_ε – Schmidt number for the kinetic energy dissipation rate
σ_t – Schmidt number for the energy equation
τ – time

References

[1] ANSYS Release 7.1, Code by ANSYS, Inc., Southpointe 275 Technology Drive, Canonsburg, PA 15317.

[2] Barron R.F., *Cryogenic heat transfer*, Ann Arbor, MI, 1999.

[3] Blanco E., Calzas C., Casas J., Gomes P., Knoops S., Serio L., Van Weelderen R., *Experimental validation and operation of the LHC test String2 cryogenic system*, Presented at CEC/ICMC (2003), Anchorage, USA, 2003.

[4] Chorowski M., *Transient behaviour and helium recovery in the LHC cryogenic system following magnet resistive transitions*, LHC Project Note 77, 1997.

[5] Chorowski M., Skoczen B., *Thermo-mechanical analysis of cold helium injection into medium-pressure (MP) gas storage tanks following resistive transition of a LHC sector*, LHC Project Note 119, 1997.

[6] *Handbook of cryogenic engineering*, Edyted by J.G. Weisend II, 1998.

[7] HEPAK Version 3.4, code by Cryodata, Inc., P.O. Box 173, Louiaville, CO 80027-0173

[8] Hees W., private communication.

[9] Lebrun Ph. *Cryogenic systems*, CAS CERN Accelerator School 1988 Proceedings, Superconductivity in Particle Accelerators, Haus Rissen, Hamburg, Germany, March1989.

[10] Mohinder L., Nayyar O.E., *Piping handbook*, McGraw-Hill, Inc, 1991.

[11] *QRL-QQS Interconnection SM type QRLAA/AD*, The LHC Project drawing No.: LHCQQSJG0003 A, Apr. 2003.

[12] *Requirements for the QRL service and return modules*, The LHC Project document No.:, LHC-QRL-NOT-1316 rev 1.2

[13] Skoczen B., *Stability, fatigue and optimization of thin-walled structures under cryogenic conditions, Application in the structural design of colliders and cryogenic transfer lines*, The LHC Division Rapport, CERN, Geneva 2001.

[14] *Supply and installation of five cryogenic interconnection boxes for the LHC,* The LHC Project document No.: LHC-QUI-CI-0001, Nov. 2000.

Appendix A

Appendix A gives the comparisons of the helium property values obtained from FLOTRAN gas model [1] and the helium property values obtained from HePak ver. 3.4 [7] at temperatures between 15 and 300 K.

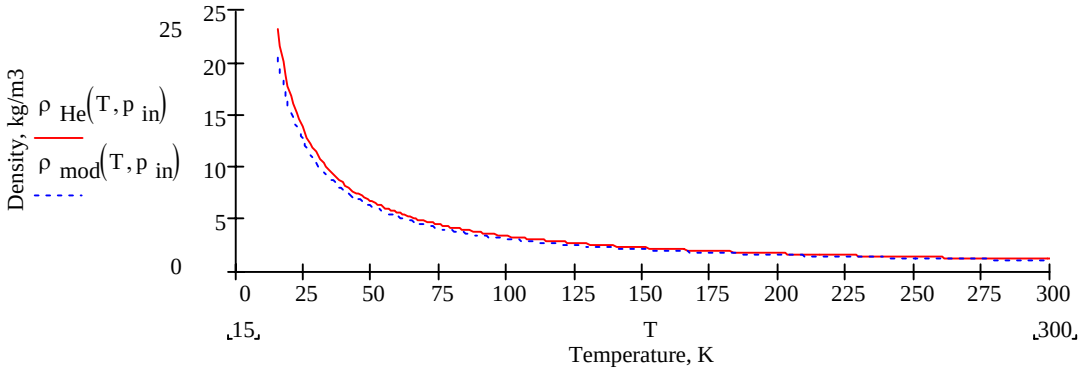

Figure A1 Helium and model gas density versus temperature

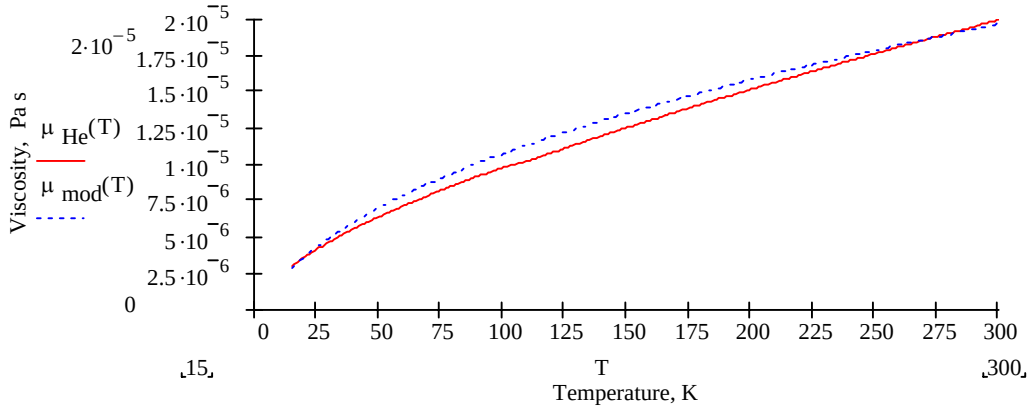

Figure A2 Helium and model gas viscosity versus temperature

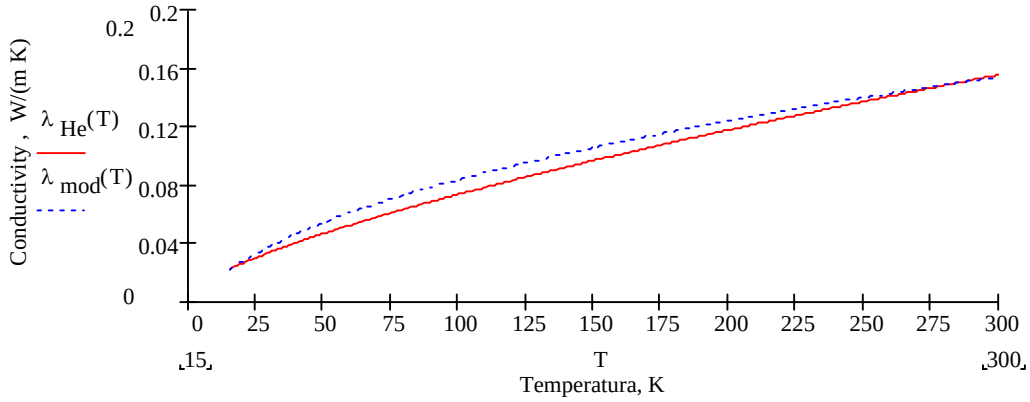

Figure A3 Helium and model gas conductivity versus temperature

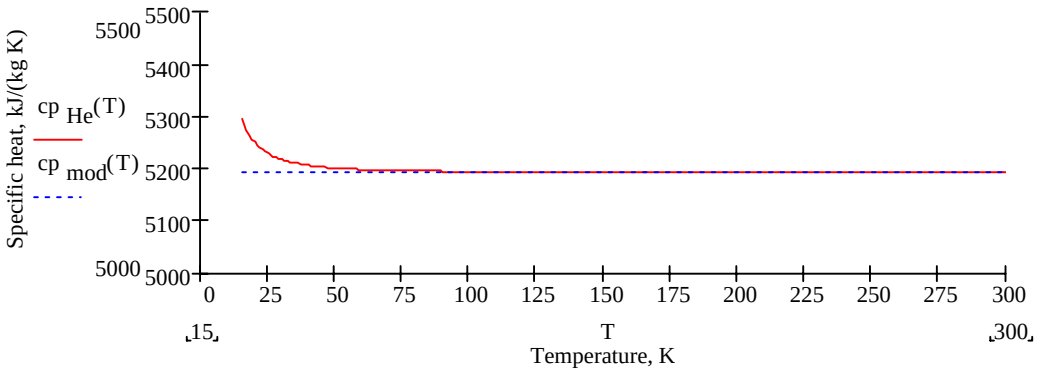

Figure A3 Helium and model gas specific heat versus temperature

Appendix B

Austenitic stainless steel AISI 304L thermal and mechanical properties at temperatures between 4 and 300 K

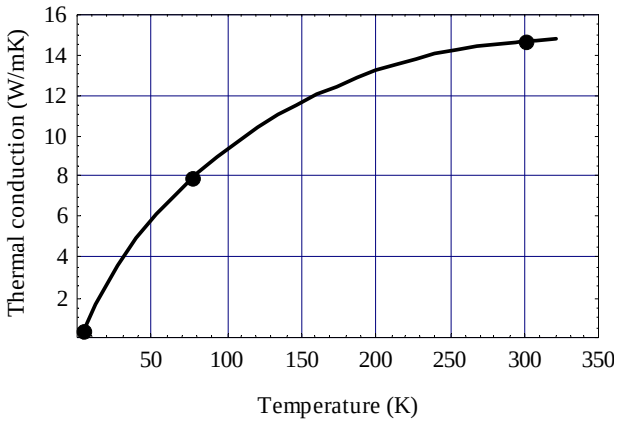

Figure B1 Thermal conductivity for austenitic stainless steel AISI 304L versus temperature [6]

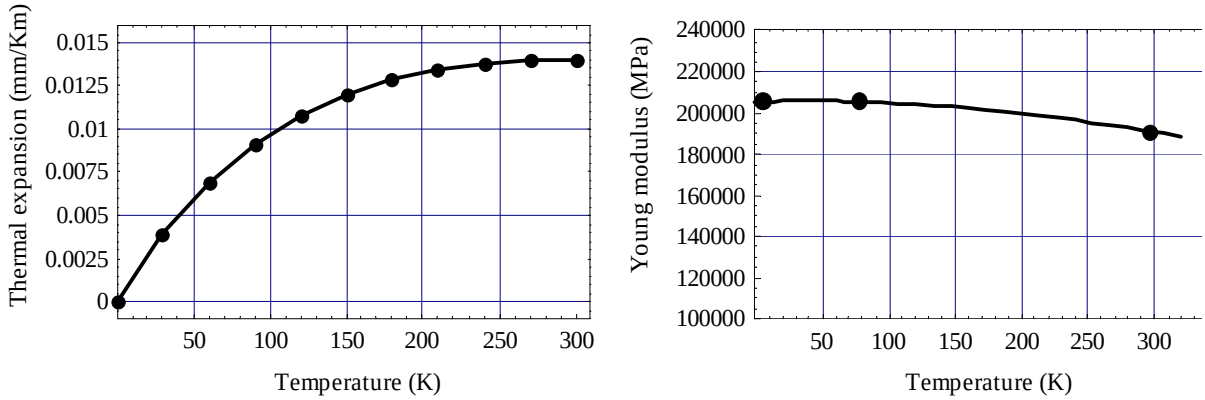

Figure B2 Thermal expansion [9] and Young modulus [13] for austenitic stainless steel AISI 304L versus temperature

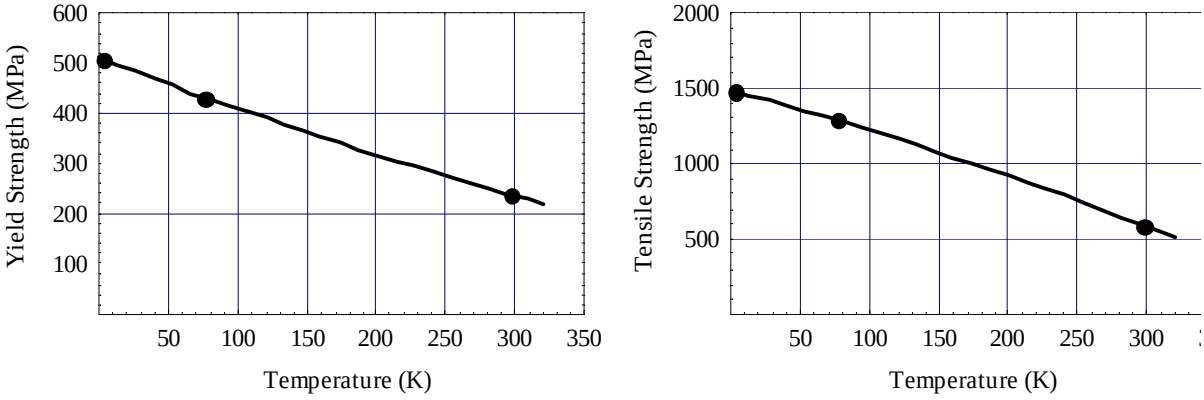

Figure B3 Yield Strength and Tensile Strength for austenitic stainless steel AISI 304L versus temperature [13]